EXPERIMENTAL INVESTIGATION OF AN OSCILLATING AIRFOIL IN THE PRESENCE OF DOWNSTREAM-GENERATED AERODYNAMIC GUSTS

M. Nowinski, P. Ott, and A. Bölcs
Swiss Federal Institute of Technology
EPFL-DGM-LTT
Lausanne, Switzerland
Fax: +41 21 693 35 02, E-mail: matthew.nowinski@erols.com

KEY WORDS: aeroelasticity, forced response, high cycle fatigue

ABSTRACT

An experimental investigation was conducted in which the unsteady aerodynamic response of a single airfoil was measured in the presence of downstream-generated aerodynamic gusts, a forced plunging motion, and a combined vibration-gust excitation. In addition, the results of these experiments were compared with 2-D, Euler computations. These efforts were aimed at evaluating the linearity of the forced response problem over a wide range of flow conditions. The results of this investigation demonstrate that the simultaneous, combined vibration-gust excitation of the airfoil can be accurately represented by a linear superposition of the individual vibration-induced and gust-induced unsteady flow fields. Based on these findings, this linear approach was applied to the available experimental data in order to characterize the aerodynamic damping contribution to the forced response loading of the airfoil.

INTRODUCTION

High cycle fatigue (HCF) due to flow-induced vibrations is a growing problem in turbomachinery. Such vibrations are typically associated with either flutter or forced response. Flutter is a self-excited phenomenon in which the unsteady aerodynamic forces on the blade are generated solely by the blade motion. Forced response involves an external, periodic flow disturbance that is completely independent of the resulting elastic blade response. In this case, the blade motion-induced aerodynamics contribute to the overall damping of the blade.

The current research in this field is primarily focused on developing accurate and efficient methods to predict such flow-induced vibrations. For forced response, both analytical and experimental studies have traditionally adopted a decoupled approach, dividing the problem into two separate components: (1) the unsteady aerodynamic loading generated on a fixed blade due to a periodic flow disturbance, and (2) the aerodynamic damping exerted on a blade vibrating in uniform flow. The complete unsteady aerodynamic loading of the blade is then quantified assuming a simple superposition of (1) and (2).

Recently, closer attention has been focused on evaluating the validity of such a linearized approach. Poensgen and Gallus (1991) and Frey and Fleeter (1999) investigated the unsteady pressures produced on a vibrating blade in the presence of upstream-generated aerodynamic gusts. A primary objective of these studies was to determine whether the unsteady aerodynamic loading of the blade resulting from a combined, simultaneous vibration-gust excitation could be represented by a linear superposition of the individual gust and blade vibration aerodynamics. In general, both studies demonstrated relatively good agreement between the measured unsteady pressure data for the combined and superimposed cases. Frey and Fleeter (1999) found that the linearity assumption was most appropriate for small blade oscillation amplitudes and low steady blade loading. Neither study addressed forced response interactions due to downstream-generated gusts, nor did they investigate the effects of reduced frequency, shocks, or off-design flow conditions, such as those involving flow separation.

The current investigation represents the continuation of a previous work (Nowinski, Ott, and Bölcs, 1997). The primary objective of both studies is to address the validity of the assumptions inherent in linearized treatments of the forced response problem. These studies are based on the measured aerodynamic response of a single airfoil to (1) downstream-generated aerodynamic gusts, (2) an imposed plunging motion, and (3) a simultaneous, combined vibration-gust

excitation. In the present paper, the linear superposition principle is evaluated over a wider range of flow conditions than investigated previously, including high flow incidence cases involving separated flow. In addition, the experimental results are compared with computational predictions obtained using a 2-D, Euler code.

EXPERIMENTAL FACILITY AND DATA ANALYSIS

In this section, a brief description of the experimental facility, test article, and data analysis techniques is provided. Additional details can be found in Nowinski, Ott, and Bölcs (1997). The experimental measurements were conducted in the Unsteady Wind Tunnel at the Ecole Polytechnique Fédérale de Lausanne (EPFL). This is a continuous flow, open cycle test facility with a rectangular test section measuring 200 mm (height) by 40 mm (width). A schematic of the facility is provided in Figure 1.

The test article consists of a single compressor blade with a NACA 3506 profile, as shown in Figure 2. The blade is suspended in the test section by an externally mounted support. An attached, hydraulically-actuated excitation mechanism can be used to impose a periodic, plunging blade motion. The blade entry into the test section is equipped with a labyrinth-type sealing, which facilitates the free movement of the blade while minimizing the leakage flow entering the test section from the exterior. In addition, a tip gap of 0.5 mm exists between the blade tip and the outer sidewall.

Approximately 400 mm downstream of the blade, a rotating device is placed in the flow path to generate upstream-running, periodic, aerodynamic disturbances. This device consists of a flat plate measuring 15 mm (height) by 39 mm (width) that is mounted within a 10 mm diameter axis driven by a hydraulic motor. Using a PC-based control system, unsteady measurements can be obtained in the presence of the vibrating blade, the downstream-generated aerodynamic gusts, or a combination of the two with a common excitation frequency and fixed phasing.

The steady aerodynamic blade loading is quantified using a series of 18 blade surface static pressure taps aligned along the blade midspan. The time-dependent, aerodynamic blade loading is based on measurements obtained using 8 high-response, piezoresistive pressure transducers embedded in the blade. The transducer locations, aligned along the blade midspan, are shown in Figure 2. In addition, the blade is equipped with a miniature accelerometer to measure the instantaneous blade position for those test cases involving the forced vibration of the blade. Time-dependent pressures are also obtained along the test section sidewall adjoining the blade tip. Of particular importance are two vertically aligned unsteady pressure taps, spaced by 40 mm, which are located approximately 100 mm downstream of the blade mid-chord. These signals serve as references to quantify the incoming, downstream-generated aerodynamic gusts.

The analog voltage signals derived from the pressure transducers and the embedded accelerometer are treated through a chain of filters and amplifiers, and subsequently digitized and stored. The signal digitization is controlled by an external trigger associated with the corresponding source of imposed excitation. For this investigation, exactly 32 data samples per excitation cycle were obtained, over a time period corresponding to approximately 400 excitation cycles. An ensemble averaging of the resulting data set is applied such that the data for a given channel is overlaid into a single reference period, effectively suppressing signal content not related to the imposed excitation frequency. A Fast Fourier Transform (FFT) decomposition is applied to the average signal and the harmonics associated with the reference frequency are extracted. The transducer and accelerometer sensitivities, and any other calibration corrections are applied to these average values. The standard deviations for each data set are calculated using the average and individual cycle values. The 95% confidence intervals are calculated from the standard deviation estimates assuming a Student's t-distribution. For the unsteady measurements, typical 95% confidence intervals are on the order of ±2% for the unsteady pressure amplitude, and ±3° for the unsteady pressure phase angle.

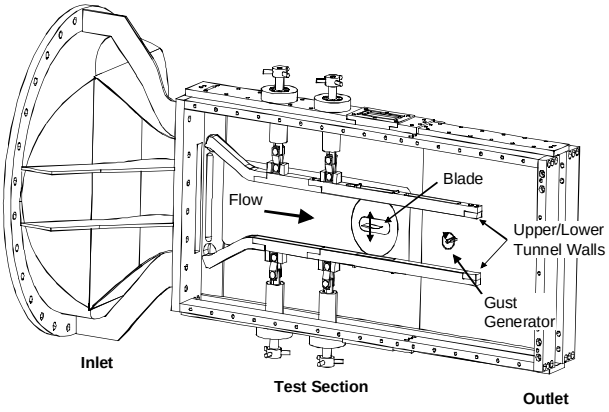

Figure 1. Unsteady Wind Tunnel Test Facility

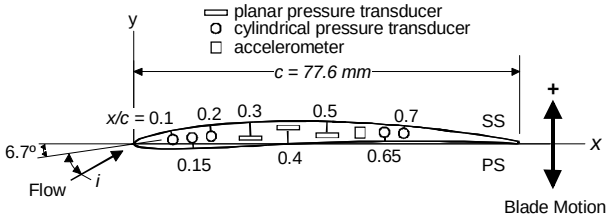

Figure 2. NACA 3506 Blade Geometry and Unsteady Instrumentation

COMPUTATIONAL PROGRAM

The computational results presented in this paper were obtained using a finite-difference code developed by Ott (1992) called INST. The INST code is based on the conservative form of the two-dimensional, time-dependent Euler equations. A solution to these equations is obtained using an explicit, second order accurate, finite-difference method. The time integration is performed using either a MacCormack predictor-corrector method or a four-step Runge-Kutta method, and the spatial integration is accomplished using an upwind scheme based on van Leer's flux vector splitting method. Examples in the literature demonstrating the application of this code to various turbomachinery-related flows include Ott, Bölcs, and Fransson (1995) and Ott, Norryd, and Bölcs (1998).

The standard INST code is configured for flows through

turbomachinery cascades. It applies capacitive-type boundary conditions at the cascade inlet and exit, and periodic boundary conditions along the upper and lower limits of the computational domain. Along the inlet boundary, the total pressure, total temperature, and flow angle are specified. Along the outlet boundary, the static pressure is prescribed. For the flow through the Unsteady Wind Tunnel, the upper and lower periodic boundaries were replaced with horizontal wall boundaries, representative of the upper and lower tunnel walls. An H-mesh was then constructed based on the test section geometry consisting of 140 x 40 points.

For the unsteady test cases involving blade vibration, the movement of the blade is captured in the INST computation by a deformation of the surrounding grid. At each time step, the blade is displaced according to a simple sinusoidal function and the computational grid is recalculated. For cases involving the downstream aerodynamic gust, a periodically time-varying outlet static pressure profile is prescribed along the exit boundary of the computational domain. For a given moment in time, the instantaneous static pressure amplitude is prescribed uniformly along this boundary (i.e. vertically planar disturbance). This is in keeping with the measured characteristics of the incoming disturbance, as will be described in the discussion of the experimental results. Finally, for the combined excitation cases, the blade motion and periodically varying downstream static pressure are prescribed simultaneously. The phasing between these excitations is also set as an input parameter according to the corresponding experimental test case.

RESULTS

Definitions

The unsteady pressure measurements are presented in terms of the unsteady pressure coefficient:

$$\tilde{c}_p(t) = \frac{|\tilde{p}|}{\hat{q}(p_{T1} - p_1)} \sin(\omega t + \theta) \qquad (1)$$

where $|\tilde{p}|$ is the pressure variation amplitude corresponding to the first harmonic of the reference excitation frequency, ω. The variable $\hat{q}$ is the non-dimensional excitation amplitude whose definition is dependent on the type of unsteady measurement. For experiments involving only blade vibration, $\hat{q}$ corresponds to the non-dimensional blade vibration amplitude:

$$\hat{q} = |\tilde{h}|/c \qquad (2)$$

For experiments involving only the aerodynamic gust excitation, $\hat{q}$ corresponds to the non-dimensional amplitude of the incoming pressure disturbance:

$$\hat{q} = |\tilde{p}_G|/p_{T1} \qquad (3)$$

Finally, for the combined excitation measurements, $\hat{q}$ is given by an addition of the previous two terms:

$$\hat{q} = |\tilde{h}|/c + |\tilde{p}_G|/p_{T1} \qquad (4)$$

The variable θ in Eq. (1) is the phase angle between the unsteady pressure signal and the reference excitation signal (i.e. the blade motion signal for the blade vibration and combined excitation experiments, and the downstream, sidewall unsteady pressure signal for the aerodynamic gust measurements). For the combined excitation measurements, the gust-vibration phase angle, σ, is defined as the phase angle of the incoming aerodynamic disturbance measured relative to the blade motion. Both phase angles are defined positive when a given signal leads the reference signal.

The overall unsteady lift force exerted by the flow on the blade can be expressed in terms of the unsteady lift coefficient:

$$\tilde{c}_L = \oint (\tilde{c}_p \vec{e}_p \bullet \vec{e}_y)\, ds \qquad (5)$$

where for a given point, s, along the blade surface, $\vec{e}_p$ is the unit vector drawn in the direction of the pressure force, and $\vec{e}_y$ is the unit vector in the positive *y*-direction (and positive vibration direction).

For cases involving blade vibration, the work done by the flow on the blade can be represented as follows:

$$W = |\tilde{c}_L| \sin(\theta_L) \qquad (6)$$

where θ_L is the phase angle between the lift force and the blade vibration.

Description of Test Cases

The experimental test cases are summarized in Table 1. The steady measurements are subdivided according to inlet Mach number (M_1 = 0.4, 0.5, and 0.6 represented by the letters A, B, and C, respectively) and inlet flow incidence (i = -10º, -5º, 0º, +5º, +10º, +15º represented by the numbers 1, 2, 3, 4, 5, and 6, respectively). For each of the 18 mean flow conditions, unsteady measurements were obtained for three different imposed excitations: (1) periodic, downstream aerodynamic gusts applied to the fixed blade, (2) a forced plunging blade motion in uniform flow, and (3) a simultaneous, combined vibration-gust excitation of the blade. For tests (1) - (3), unsteady measurements were obtained for three different excitation frequencies: f = 20, 60, and 100 Hz. In addition, for the combined excitation of the blade, measurements were acquired for a minimum of 5 gust-vibration phase angles for each of the three excitation frequencies.

Table 1. Experimental Test Cases

Cases	***M₁***	***i* (º)** $\Delta i = 5^o$	***k*** f = 20, 60, 100 *Hz*
A1…A6	0.40	-10º…+15º	0.04, 0.11, 0.18
B1…B6	0.50	-10º…+15º	0.03, 0.09, 0.15
C1…C6	0.60	-10º…+15º	0.02, 0.07, 0.12

Steady Flow Measurements

A primary focus of the steady flow portion of this investigation was to identify those flow phenomena that significantly impact the unsteady flow behavior. These aspects of the flow are emphasized in the discussion below.

A typical set of steady blade surface measurements for the subsonic test cases (Cases A, B, C1, and C2) is presented in Figure 3a corresponding to Case A3 (M_1 = 0.4, i = 0º). The associated INST predictions are also provided and generally agree well with the measured values. The flow is characterized by a gradual deceleration along the suction side, and a slight

acceleration along the pressure side, from the leading edge to the trailing edge. For $i \geq +10^o$, flow separation occurs along the suction side resulting in an overall "flattening" of the isentropic Mach number distribution relative to that shown in Figure 3a. For $i = -10^o$, the suction and pressure side behavior shown in Figure 3a is essentially reversed.

An example of the transonic test cases (Cases C3-C6) is provided in Figure 3b corresponding to Case C3 ($M_1 = 0.6$, $i = 0^o$). INST computations are also shown in the plot. The agreement between the measurements and the computations is good overall, but some discrepancies exist along the suction side in the vicinity of the leading edge shock. Using Schlieren flow visualization techniques, it was observed that the shock behavior for all of the transonic cases is highly unsteady, even in the absence of any externally imposed excitation. These instabilities are particularly pronounced for the high incidence flow cases where the shocks are closely coupled with the suction side flow separation.

A series of blade surface flow visualization studies using shear-sensitive liquid crystals revealed the existence of a corner flow separation along the suction side of the blade adjoining the hub sidewall. These studies also identified a strong coupling between the corner flow separation and the small amount of leakage flow that passes through the labyrinth sealing. This interaction results in a disproportionate augmentation of both the chordwise and spanwise extent of the corner separation. For $i = 0^o$, the separated region reaches the midspan measurement positions along the latter half of the blade and continues to grow with increasing flow incidence. Its presence produces a strong mean flow contraction along the suction surface, and also affects the unsteady blade surface behavior. Additional details are provided subsequently in the discussion of the time-dependent results.

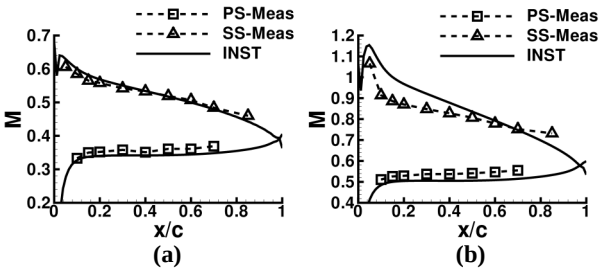

Figure 3. Steady Blade Surface Measurements: (a) Case A3, (b) Case C3

Downstream Aerodynamic Gust Unsteady Response

The aerodynamic gusts produced by the downstream gust generator are primarily static pressure perturbations, which travel upstream at the isentropic wave speed, a-U, and are both vertically aligned and of uniform amplitude upon arriving in the test section. These characteristics were verified using quasi-steady measurements, time-dependent sidewall pressure measurements, as well as Navier-Stokes computations of the flow around the rotating device (Grüber and Carstens, 1996). The specific details of this portion of the investigation, however, are not presented in this paper, but can be found in Nowinski, 1999.

An example of the measured unsteady aerodynamic response of the fixed blade to the downstream gusts is provided in Figure 4 for Case A3, $f = 100$ Hz, $k = 0.18$. The corresponding INST computations are also shown in the plot. Overall, it was found that the unsteady response of the blade for subsonic flow is basically quasi-steady in nature. This was determined by comparing the unsteady results with the measured variation of the mean static pressure along the blade surface in response to stepwise clocking of the downstream flat plate. This quasi-steady behavior is characterized by a close trendwise agreement between the pressure variation amplitude and mean Mach number distributions along the blade. These similarities can be seen by comparing Figure 4 and Figure 3a.

Experimentally, such quasi-steady behavior is most pronounced for lower excitation frequencies. In general, the comparison between computation and experiment is also best for these cases. With increasing f (and k), the measured $|\tilde{c}_p|$ distributions tend to "flatten out", and the difference between the upper and lower unsteady pressure amplitudes is diminished. Such frequency-dependent behavior, however, is much less pronounced in the INST calculations, resulting in the discrepancies observed in Figure 4.

With regards to the unsteady pressure phase angle, the expected behavior is perhaps best illustrated by the INST calculations in Figure 4. Namely, the incoming gust enters the test section from downstream and propagates upstream along the blade surface (hence, the positively sloped θ vs. x/c curves in Figure 4), but with the suction side disturbance lagging that along the pressure side (a-U_{SS} < a-U_{PS}). Along the pressure side, the measurements agree well with the INST predictions. Along the suction side, however, the measured flow disturbance generally *leads* that along the pressure side. This behavior is in contrast to the idea of a simple upstream running, isentropic wave, and these effects could result from the presence of the corner flow separation over the latter half of the blade for this test case. Interestingly, a series of unsteady pressure measurements obtained along the sidewall of the test section adjoining the blade tip (not shown here) demonstrated a similar suction side behavior.

For the transonic test cases, the unsteady aerodynamic response of the blade to the downstream aerodynamic gusts is dominated by the suction side shock(s). An example of these measurements, along with the corresponding INST calculations, is provided in Figure 5 for Case C3, $f = 100$ Hz, $k = 0.15$. With regards to the unsteady pressure amplitude, the agreement between measurement and calculation is generally good. The location of the shock is indicated by a sharp peak in the computed unsteady pressure amplitude at $x/c = 0.08$ along the suction side. The first unsteady measurement position ($x/c = 0.1$) is slightly downstream of this location and instead exhibits an abrupt drop in $|\tilde{c}_p|$. This behavior is typical of the measured transonic test cases and could indicate the existence of a shock-induced boundary layer separation in this region. As would be expected in such a case, there is no evidence of this $|\tilde{c}_p|$ drop in the Euler-based INST computations. With increasing flow incidence, the shock moves farther downstream along the blade, and the first unsteady measurement location also exhibits a $|\tilde{c}_p|$ peak similar to the computed behavior shown in Figure 5. With regards to the unsteady pressure phase angle, once again the agreement is good between measurement and calculation along the pressure side, but along the suction side the measured phase angle

generally leads that along the pressure side.

The time-dependent loading of the blade due to the aerodynamic gusts can be obtained by integrating the unsteady pressures measured along the blade surface, according to Eq. (6). In Figure 6, $(|\tilde{c}_L|)_G$ is plotted as a function of k and i. The black dots in the plot indicate the test cases used to construct the contours. The highest unsteady blade loading is generally associated with lower values of k (< 0.08) and positive flow incidences. This trend can be attributed to the tendency for the difference between the unsteady amplitudes along the pressure and suction sides to decrease with increasing k, as mentioned previously. The peak $(|\tilde{c}_L|)_G$ values occur near k = 0.05, i = +15°. The lowest unsteady blade loading generally occurs for i < 0°, where the unsteady blade surface pressure distribution approaches that of a flat plate (i.e. there is little or no overall unsteady pressure difference across the blade).

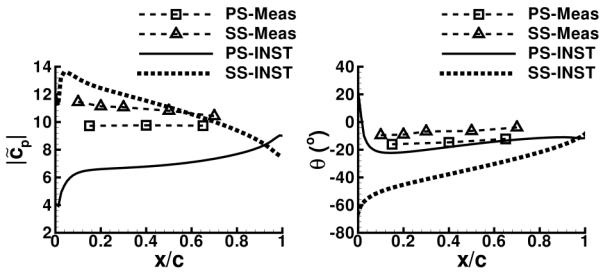

Figure 4. Blade Surface $\tilde{c}_p$ (Case A3, *f*=100Hz)

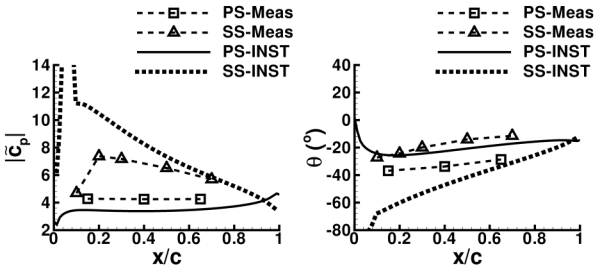

Figure 5. Blade Surface $\tilde{c}_p$ (Case C3, *f*=100Hz)

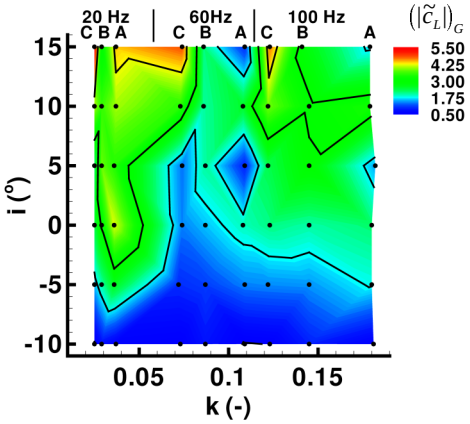

Figure 6. Aerodynamic Gust Response Loading, $(|\tilde{c}_L|)_G$

Oscillating Blade Unsteady Response

A series of experiments was conducted to quantify the time-dependent aerodynamic response of the blade when forced to vibrate in uniform flow. An example of this response is provided in Figure 7 for Case A3, f = 100 Hz, k = 0.18, along with the corresponding INST computations. This case is representative of the subsonic test case results. In general for these test cases, the unsteady pressure amplitudes decrease from the leading edge to the trailing edge along both the pressure and suction sides. In addition, the average unsteady pressure phase angle along the pressure and suction sides differs by approximately 180°.

For Case A3, the agreement between the measured $|\tilde{c}_p|$ distribution and the INST calculations is good. For the θ distributions, the agreement is good across the pressure side, but becomes progressively worse along the suction side toward the trailing edge. These differences tend to become more pronounced with increasing flow incidence. The location of these discrepancies along the blade, as well their dependency on inlet flow incidence, points to the presence of the hub corner flow separation, described previously, as a likely cause. Furthermore, as this flow separation is highly influenced by the leakage flow through the labyrinth sealing, these effects could be amplified due to a coupling with the blade motion.

For the transonic test cases, as observed for the aerodynamic gust measurements, the unsteady response of the blade to the forced vibration is dominated by the suction side shock(s). An example of these measurements and the corresponding INST calculations is provided in Figure 8 for Case C3, f = 100 Hz, k = 0.15. The location of the shock is indicated by a sharp peak in the computed unsteady pressure amplitude near x/c = 0.08 along the suction side. Once again, there is evidence in the measurements of a drop in unsteady pressure amplitude just downstream of the mean shock position. Overall the agreement between the measured and computed unsteady pressure amplitudes is fair. For the phase angle, similar trends to those described above for the subsonic cases were observed.

The time-dependent loading of the blade due to the forced vibration is expressed in Figure 9 in terms of the aerodynamic work input, W_V, plotted as a function of k and i. For flutter, the sign of W_V determines the aerodynamic stability of the blade. This term is traditionally referred to as the aerodynamic damping coefficient, Ξ, where $\Xi = -W_V$. A negative value of Ξ or positive value of W_V indicates a flow condition susceptible to flutter phenomena. Two regions of positive work input appear for k < 0.05, near $-5° < i < 0°$ and $+10° < i < +15°$, as indicated by the thick black contours. Outside of these regions, the blade is aerodynamically damped. With a few exceptions near i = +5, the work input for the measured cases generally becomes more negative (more damped) with increasing reduced frequency.

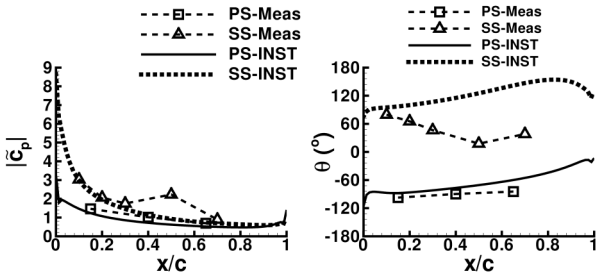

Figure 7. Blade Surface $\tilde{c}_p$ (Case A3, *f*=100Hz)

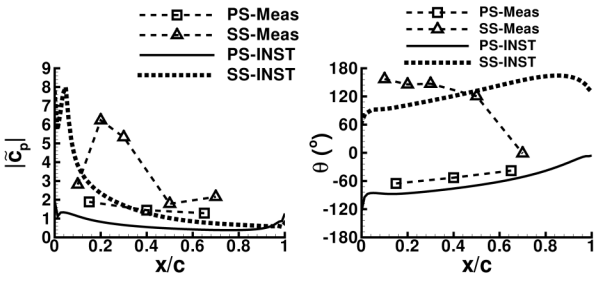

Figure 8. Blade Surface $\tilde{c}_p$ (Case C3, *f*=100Hz)

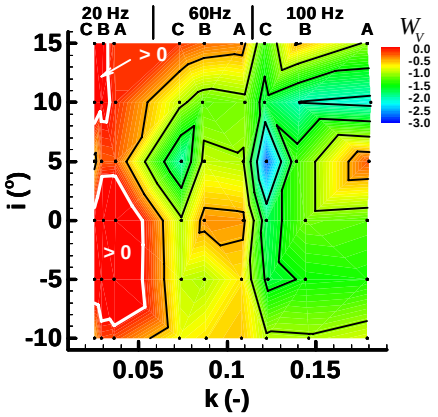

Figure 9. Forced Vibration Aerodynamic Work, W_V

Combined Vibration-Gust Excitation Unsteady Response

A series of experiments was conducted to quantify the time-dependent aerodynamic response of the blade to a simultaneous, combined forced vibration-downstream aerodynamic gust excitation. The primary objective of this effort was to determine whether the combined, unsteady aerodynamic response of the blade could be accurately represented by a linear superposition of the individual vibration-induced and gust-induced responses.

The applicability of this linearization is evaluated here for three different flow conditions: (1) attached, subsonic flow, Case A3; (2) separated, subsonic flow, Case A5; and (3) transonic flow involving a leading edge shock along the suction side of the blade, Case C3. These evaluations are made based on the blade surface unsteady pressures measured at midspan.

The results for Case A3 for $f = 100$ Hz and a gust-vibration phase angle, σ, of -97° are shown in Figure 10. In this plot, two sets of data are presented, one corresponding to the measured unsteady pressures for the simultaneous, combined vibration-gust excitation of the blade, denoted by "C", and another corresponding to the linear superposition of the individual downstream aerodynamic gust and blade vibration cases, denoted by "G+V". From Figure 10, it can be seen that the agreement between the two sets of data, with regards to both the unsteady pressure amplitude and phase angle, is excellent. This level of agreement is typical of the other attached, subsonic flow cases, independent of excitation frequency or gust-vibration phase angle. Corresponding INST-based comparisons also demonstrated a similar level of agreement.

The results for Case A5, $f = 100$ Hz, $\sigma = -60°$ are shown in Figure 11. Once again, the agreement between the simultaneous and superimposed values is very good, despite the presence of a severe flow separation along the suction surface of the blade. In general, it was observed that the presence of separated flow, whether global ($i \geq +10°$) or localized (the hub corner flow separation) has little effect on the linearity of the combined vibration-gust excitation aerodynamic response.

The results for Case C4, $f = 100$ Hz, $\sigma = +2°$ are shown in Figure 12. Overall, the agreement between the simultaneous and superimposed blade surface unsteady pressures is good. However, some relatively significant discrepancies appear in the leading edge region along the suction side near the shock. The difference in unsteady pressure amplitude at this location is approximately 40%, and more than 60° for the phase angle. Such large discrepancies, however, are not consistently evident for the different tests conducted for Case 4. This behavior points to the possibility that these non-linearities are in fact limited to a highly localized region around the shock itself.

Support for this idea is provided by the INST computations corresponding to Case C4, $f = 100$ Hz, $\sigma = +2°$, shown in Figure 13. In this plot, the lines are representative of the actual calculated locations along the blade. The symbols shown in the plot are only placed every 5th node in order to preserve its overall readability. First, it should be noted that the mean shock location for the computed case is farther downstream along the suction surface than in the measurements. This makes a direct comparison between Figure 13 and Figure 12 difficult. In Figure 13, the presence of the shock is indicated by the large peak in the computed unsteady pressure amplitude distributions near $x/c = 0.25$. Away from the shock, the agreement between the simultaneous and superimposed results is excellent. Near the shock, it can be seen that the agreement remains good up to a small region surrounding the mean shock location. In this region, there are significant discrepancies with regards to both the unsteady pressure amplitude and phase angle. The localized nature of these differences, however, would tend to minimize their effect on integrated quantities, such as the unsteady lift or work. In this context, therefore, the non-linearities near shocks do not significantly influence the applicability of the superposition principle.

The above examples demonstrate clearly that the simultaneous, combined blade vibration-downstream aerodynamic gust excitation can be accurately represented by a linear superposition of the individual vibration and gust

excitation unsteady flow fields. Based on these findings, this linearized approach can be used with confidence to expand on the available measured, combined excitation data. In the following discussion, the linear superposition principle is applied to characterize the importance of the aerodynamic damping on the gust-induced loading of the blade from a forced response perspective.

The unsteady lift exerted on the fixed blade due to the downstream-generated gust was presented as a function of reduced frequency and incidence in Figure 6. It is now assumed that the blade is free to respond in an elastic sense to this flow disturbance. Referring to Eq. (6), the maximum work input into the blade occurs when the phase of the unsteady lift force leads the blade motion by +90º. From this perspective, the results plotted in Figure 6 can also be interpreted as a representation of the maximum work done by the downstream aerodynamic gust on the blade. This representation, however, ignores the aerodynamic effects associated with the blade motion. Using this case as a reference, the contribution of the aerodynamic damping to the overall forced response loading of the blade is illustrated below.

The linear superposition principle is applied here in terms of the aerodynamic work input into the blade, as shown below:

$$W_{G+V} = W_G^{Max} + W_V \qquad (7)$$

where W_G^{Max} is the maximum aerodynamic work done by the aerodynamic gust (i.e. $(\theta_L)_G = 90^o$, Figure 6), W_V is the aerodynamic work done on the blade due to its motion (refer to Figure 9), and W_{G+V} is the work done due to the combined vibration-gust excitation of the blade.

Figure 14 plots the percent difference between the combined excitation work input, W_{G+V}, and the maximum gust only work input, W_G^{Max}, as a function of reduced frequency and flow incidence. Overall, it can be seen that the aerodynamic damping contribution, as expected, tends to reduce the overall energy input into the blade.

The bold black lines in Figure 14 represent the contour corresponding to a 100% reduction in the aerodynamic work input. The regions enclosed by these lines are where the aerodynamic damping of the blade is actually greater than the maximum work done by the aerodynamic gust. Without any positive work input into the blade, however, no elastic blade response is possible. Hence, this is a non-physical situation made possible by the fact that the blade vibration is forced in these tests.

The white lines in Figure 14 represent the contour corresponding to a value of 0%. The regions enclosed by these contours are where the aerodynamic work input into the blade has in fact increased with the addition of the aerodynamic damping effects (i.e. negative damping). By definition for forced response, the aerodynamic damping of the blade should be positive. Hence, these regions would be more likely associated with the occurrence of flutter phenomena. Not surprisingly, these regions of work increase correspond to those aerodynamically unstable areas described in Figure 9.

In conclusion, it can be seen that the consideration of the aerodynamic damping results in significant changes in the overall work done by the imposed aerodynamic gusts on the moving blade. In the context of the forced response problem, this demonstrates the importance of considering this contribution to obtain accurate estimations of the resulting unsteady blade loading and elastic blade response. Also, an example has been provided of how the linear superposition principle can be applied to quantify the complete forced response loading of the blade.

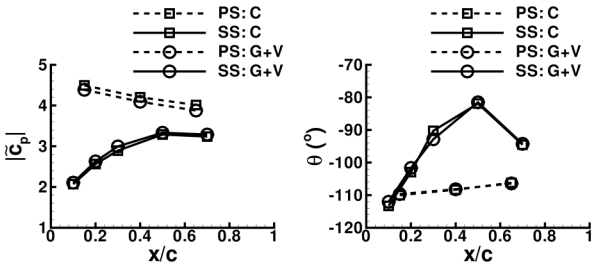

Figure 10. Measured Unsteady Blade Surface Pressures (Case A3, *f*=100 Hz, σ =-97º)

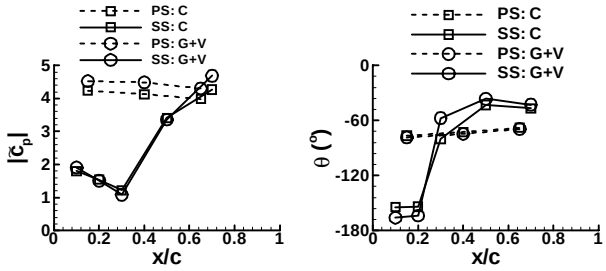

Figure 11. Measured Unsteady Blade Surface Pressures (Case A5, *f*=100 Hz, σ =-60º)

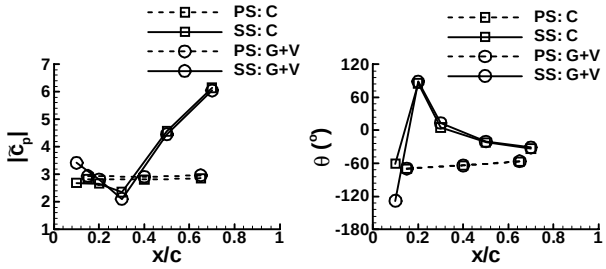

Figure 12. Measured Unsteady Blade Surface Pressures (Case C4, *f*=100 Hz, σ =+2º)

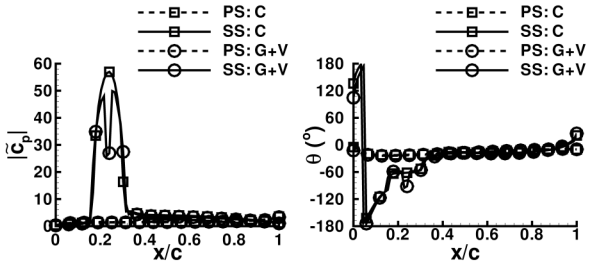

Figure 13. Computed Unsteady Blade Surface Pressures (Case C4, *f*=100 Hz, σ =+2º)

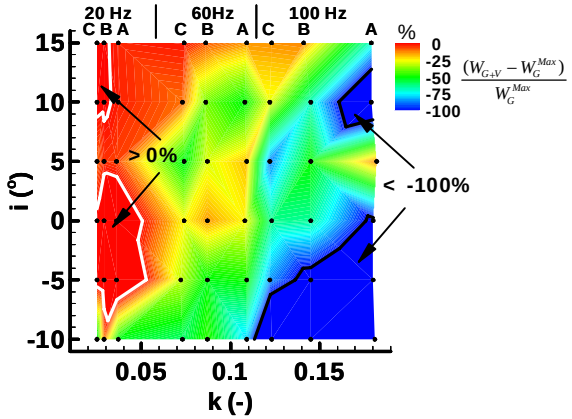

Figure 14. Difference in Work Input between Combined Vibration-Gust Excitation and Aerodynamic Gust Cases, $\left((W_{G+V} - W_G^{Max}) / W_G^{Max}\right)$

SUMMARY AND CONCLUSIONS

Experiments were conducted in which the unsteady aerodynamic response of a single airfoil was evaluated for three different cases: (1) the fixed airfoil subjected to periodic, downstream-generated aerodynamic gusts, (2) the airfoil forced to vibrate in uniform flow, and (3) the airfoil forced to vibrate in the presence of the downstream aerodynamic gusts.

These experiments demonstrated that the unsteady aerodynamic response of the airfoil depends on a number of parameters, including the inlet Mach number, inlet flow incidence, and reduced frequency. In the case of the combined vibration-gust excitation, the gust-vibration phase angle plays a critical role as well. Furthermore, it was determined that the simultaneous, combined forced vibration-downstream aerodynamic gust excitation of the airfoil can be accurately predicted by the linear superposition of the individual gust-induced and vibration-induced unsteady flow fields. This principle was shown to be applicable to a wide range of flow conditions, including those involving separated flow. The only significant discrepancies were observed in the presence of shocks, but these non-linearities were limited to a localized region around the mean shock location.

Through comparisons with the experimental measurements, it was shown that a 2-D, Euler code is generally sufficient to predict the unsteady aerodynamic behavior of the airfoil in response to downstream aerodynamic gust, forced vibration, and combined vibration-gust excitations. As expected, limitations of the code's applicability were identified for cases involving strong shocks, flow separation, or 3-D flow phenomena, such as the corner flow separation observed during the experimental investigation.

NOMENCLATURE

c	chord length
f	frequency
$\lvert\tilde{h}\rvert$	blade vibration amplitude
i	inlet incidence angle
k	reduced frequency, $\omega c/2U_1$
$\lvert\tilde{p}_G\rvert$	downstream aerodynamic gust amplitude
PS	pressure side of the blade
p_{T1}	inlet total pressure
p_1	inlet static pressure
SS	suction side of the blade
t	time
U_1	inlet velocity
W	non-dimensional work
σ	gust-vibration phase angle
θ	unsteady pressure phase angle
θ_L	unsteady lift force phase angle
Ξ	aerodynamic damping coefficient

Subscripts

1	inlet flow property
2	outlet flow property
C	simultaneous, combined vibration-gust excitation
G	aerodynamic gust
G+V	superimposed vibration-gust excitation
V	blade vibration

Superscripts

Max	maximum value

REFERENCES

Frey, K. K., and Fleeter, S., 1999, "Combined-Simultaneous Gust and Oscillating Compressor Blade Unsteady Aerodynamics," ASME Paper 99-GT-414.

Grüber, B., and Carstens, V., 1996, "Computation of the Unsteady Transonic Flow In Harmonically Oscillating Turbine Cascades Taking Into Account Viscous Effects," ASME Paper 96-GT-338.

Nowinski, M., 1999, "Experimental Investigation of an Oscillating Airfoil in the Presence of Downstream Generated Gusts," Ph.D. Dissertation, Swiss Federal Institute of Technology, Lausanne, Switzerland.

Nowinski, M., Ott, P., and Bölcs, A., 1997, "A Basic Forced Response Experiment," in "Unsteady Aerodynamics and Aeroelasticity of Turbomachines: Proceedings of the 8th International Symposium held in Stockholm, Sweden, 14-18 September 1997," Torsten H. Fransson, ed., Kluwer Academic Publishers, Dordrecht, The Netherlands, ISBN 0-7923-5040-5.

Ott, P., 1992, "Oszillierender Senkrechter Verdichtungsstoss In Einer Ebenen Düse," Communication du Laboratoire de Thermique Appliquée et de Turbomachines de l'Ecole Polytechnique Fédérale de Lausanne, No. 18.

Ott, P., Bölcs, A., and Fransson, T. H., 1995, "Experimental and Numerical Study of the Time-Dependent Pressure Response of a Shock Wave Oscillating in a Nozzle," Journal of Turbomachinery, Vol. 117, No. 1, January, pp. 106-114.

Ott, P., Norryd, M., and Bölcs, A., 1998, "The Influence of Tailboards on Unsteady Measurements in a Linear Cascade," ASME Paper 98-GT-572.

Poensgen, C. A., and Gallus, H. E., 1991, "Experimental Investigation on the Unsteady Pressure Field on a Vibrating Cascade in Unsteady Flow," presented at Unsteady Aerodynamics of Turbomachines and Propellers, University of Notre Dame, Indiana, September 15-19, pp. 583-601.